IJE TRANSACTIONS A: Basics Vol. 36 No. 10, (October 2023) 1815-1826

International Journal of Engineering

Journal Homepage: www.ije.ir

Numerical Simulation of Fiber-reinforced Concrete under Cyclic Loading using Extended Finite Element Method and Concrete Damaged Plasticity

S. El Yassari*, A. EL Ghoulbzouri

MODSGC Unit, National School of Applied Sciences Al Hoceima, University Abdelmalek Essaadi, Tangier, Morocco

P A P E R I N F O

Paper history:
Received 02 June 2023
Received in revised form 27 June 2023
Accepted 28 June 2023

Keywords:
Fiber Reinforced Concrete
Cyclic Loading
Concrete Damage Plasticity
Steel Fiber
Polypropylene Fiber
Extended Finite Element Method

A B S T R A C T

In recent years, the scientific community has shown a growing interest in fiber-reinforced concrete (FRC) for modern structures due to its enhanced ductility compared to traditional reinforced concrete (RC). This paper introduces an analytical model that incorporates a comprehensive fiber reinforcing index (RI) to study various types of FRC. The analysis focuses on the compressive and tensile behaviors, damage evolution under cyclic loading, and crack propagation in the concrete matrix. To effectively simulate crack initiation and propagation in FRC structures, the extended finite element method (XFEM) is employed, leveraging its fracture-solving capabilities. Additionally, the XFEM is combined with the concrete damaged plasticity (CDP) modeling approach to examine the quasi-static and hysteretic performance of FRC columns. Three-dimensional nonlinear finite element models are constructed using the commercial software Abaqus. These models incorporate steel fibers, polypropylene fibers, and a combination of both types of fibers in the FRC structures**.** Furthermore, the accuracy of the XFEM-CDP-based analysis in predicting hysteretic behavior is validated against results from previous research articles, demonstrating reasonable accuracy. It allows engineers to accurately capture the nonlinear behavior of concrete, including cracking, crushing, and plastic deformation, while also considering the complex crack patterns, providing a better understanding of the seismic performance of FRC structures using numerical simulations.

***doi**: 10.5829/ije.2023.36.10a.08*

1. INTRODUCTION

During earthquakes, bridge columns are often the most vulnerable and deficient components, particularly when in moderate damage states [1]. Transverse stirrups in these columns are prone to deficiencies, leading to multiple damage states, ranging from concrete cracking to cover spalling, and eventually the failure of steel bars at the base of the columns.

The seismic performance of bridge columns can be significantly improved by enhancing their ductility, lateral stiffness, and energy dissipation capacity. Local increases in transverse stirrup density are the conventional method to enhance column ductility, but this approach presents challenges in construction and compromises the quality of concrete pouring [2, 3]. Consequently, fiber-reinforced concrete (FRC) has emerged as an alternative to reinforced concrete (RC), with studies showing that partial or full substitution of RC with FRC can effectively enhance structural responses and repair damaged infrastructures [4-7]. Full substitution of RC columns with FRC has been proven effective in improving ductility and seismic behavior [2, 4, 8–11].

However, experimental studies on FRC have been abundant. A few efforts have been dedicated to developing constitutive relations and numerical modeling. Experimental approaches suffer from drawbacks such as the difficulty of setting up full-scale models and limited measurement ranges for capturing important parameters like bond-slip behavior, cracking, and plastic strain. Furthermore, experimental methods are time-consuming and costly.

*Corresponding author Email: soufiane.elyassari1@etu.uae.ac.ma
(S. El Yassari)

Please cite this article as: S. El Yassari, A. EL Ghoulbzouri, Numerical Simulation of Fiber-reinforced Concrete under Cyclic Loading using Extended Finite Element Method and Concrete Damaged Plasticity, ***International Journal of Engineering, Transactions A: Basics***, Vol. 36, No. 10, (2023), 1815-1826

With the advancements in computer processing power and structural finite element theory, the finite element method has become an effective tool for analyzing the nonlinear and dynamic behavior of RC columns under seismic events. To accurately model the behavior of components such as steel reinforcements and the concrete matrix, precise and effective constitutive relationships are crucial. While constitutive models for steel have matured due to its isotropic nature, concrete presents challenges with its complex mechanical phenomena, including inelastic damage, cracking, hardening, and softening. Consequently, various analytical theories for concrete constitutive laws have been implemented in finite element programs.

The Concrete Damaged Plasticity (CDP) model, integrated with the concept of damaged elasticity, tensile and compressive plasticity, has gained research interest, particularly with the widespread use of the Abaqus software. The CDP model has shown good agreement between numerical predictions and test results for FRC behavior [12, 13]. However, CDP models only accurately predict material behavior prior to fracture initiation. One disadvantage is that these constitutive laws model material degradations and cracks in a smeared manner, failing to account for discontinuities in crack propagation and discrete cracks [14-16].

Several techniques have been proposed to address this issue. One approach is to remove elements when a damage parameter exceeds a critical value. However, this method alters the mass of the model and is sensitive to mesh configurations [15]. Cohesive crack models have also been proposed to simulate crack growth in FRC structures, considering the bridging action of aggregates and fibers. Although these models provide detailed information about concrete and fiber behavior separately, their implementation becomes challenging in complex loading cases and structures, limiting their applicability [13, 17-21].

Researchers have explored meshless methods and adaptive finite elements as alternatives [21, 22]. Cohesive crack models have been used to describe the fracture process zone in ductile and quasi-brittle materials [23, 24]. These models suppress stress and strain singularities at crack tips. Incorporating displacement jumps, XFEM allows for mesh-independent crack path determination [23]. XFEM enables smooth crack growth in finite element meshes without remeshing [23, 25]. Unlike cohesive crack models, XFEM does not require a predefined crack path, making it suitable for studying cracking behavior. However, existing XFEM models have primarily focused on predicting crack growth under monotonic loading, and the simulation of crack growth combined with material fatigue using XFEM remains unexplored.

In this paper, we propose coupling XFEM with the CDP model to simulate cyclic fatigue and cracking behavior in FRC. This combined model enables the integration of fatigue damage accumulation and crack propagation stages into a comprehensive process. Numerical results obtained using the XFEM-CDP model are validated against independent experimental data with different fiber combinations. The effectiveness and accuracy of the proposed model are demonstrated, showing improved agreement with experimental results compared to classical CDP models.

2. MATERIALS AND METHODS

2. 1. Compressive Behavior Abadel et al. [26] developed an analytical model for predicting compressive stress-strain curves of HyFRC, which quantifies the effect of each type of fiber on compressive strength and stress-strain curves in terms of a comprehensive fibre reinforcing index. The model exhibited a correlation with experimental test results. The compressive behavior σ_c model was as follows:

$$\sigma_c = \left(\frac{\beta\left(\frac{\varepsilon_c}{\varepsilon_0}\right)}{\beta - 1 + \left(\frac{\varepsilon_c}{\varepsilon_0}\right)^{\beta}} \right) f_{cu} \quad (1)$$

where f_{cu} denotes the ultimate compressive stress, ε_c and ε_0 represents the compressive strain and the strain at peak stress of plain concrete (= 0,002), respectivly.

The parameters can be calculated using the following equations:

$$\beta = 1 + 5e^{-1,376RI_v} \quad (2)$$

$$\beta_0 = 0{,}108 f_c - 0{,}966 \quad (3)$$

$$f_{cfrc} = f_{c0} + 5{,}222RI_v \quad (4)$$

$$\varepsilon_{frc} = \varepsilon_{c0} + 0{,}0004RI_v \quad (5)$$

$$RI_v = \sum RI_{vi} \quad (6)$$

$$RI_{vi} = V_i \frac{l_i}{d_i} \frac{E_i}{E_s} \quad (7)$$

For the plain concrete, the value of parameter β_0 can be calculated with the help of the Equation 3. $\mathrm{RI_v}$, $\mathrm{V_i}$, $\mathrm{l_i}$, and $\mathrm{d_i}$ denote the reinforcing index, fibers' volume fraction, length, and diameter (or their corresponding diameter in non-circular sections), $\mathrm{E_i}$ and $\mathrm{E_s}$ are the fiber's and steel material's modulus of elasticity, respectively.

2. 2. Tensile Behavior

2. 2. 1. For Plain Concrete The stress-crack opening displacement relationship adopted for plain concrete was proposed to capture the tensile behavior.

$$\frac{\sigma_t}{f_t} = \left(1 + \left(c_1 \frac{w_t}{w_{cr}}\right)^3\right) e^{\left(-c_1 \frac{w_t}{w_{cr}}\right)} - \frac{w_t}{w_{cr}}(1 + {c_1}^3) e^{(-c_1)} \quad (8)$$

$$f_t = 1{,}4\left(\frac{f_{cu}-8}{10}\right)^{2/3} \quad (9)$$

$$G_F = \left(0{,}0469{d_a}^2 - 0{,}5d_a + 26\right)\left(\frac{f_{cu}}{10}\right)^{0{,}7} \quad (10)$$

$$w_{cr} = 5{,}14\frac{G_F}{f_t} \quad (11)$$

In these equations, the f_t is the tensile strengths of plain concrete, w_t, w_{cr} denotes the crack opening displacement and crack displacement at the complete loss of tensile stress, respectivly. d_a and l_{eq} represent the maximum aggregate size of the concrete (20 mm) and the mesh element length, respectivly.

2. 2. 1. For FRC Concerning the tensile behavior of FRC, $\sigma_t(w)$, Almusallam et al. [27] proposed an analytical model to describe the tensile softening behavior based on the reinforcing index, RIv. This model was obtained through inverse analysis and provides a good agreement with experimental results.

$$\sigma_t(w_t) = a_1 f_{tfrc} e^{(-a_2 w_t)} \quad (12)$$

$$a_1 = 0{,}75 \quad (13)$$

$$a_2 = 10e^{-4{,}3RI_v} \quad (14)$$

$$f_{tfrc} = (f_t - 1) + e^{1{,}23RI_v} \quad (15)$$

where f_{tfrc} denotes the tensile strength of FRC.

It was assumed that each element in the numerical simulation had a single crack. This assumption is suitable for optimal simulations. As a result, the strain in terms of crack opening can be determined by summing the elastic strain and the crack opening and dividing it by the element length.

$$\varepsilon_t = \varepsilon_{tm} + w_t/l_{eq} \quad (16)$$

ε_{tm} is the tensile strain correspending to the tensile strengths.

2. 3. Concrete Damage Plasticity Model In this study, the behavior of steel was simulated using a uniaxial plasticity model, while a more comprehensive CDP model was employed for simulating the behavior of concrete. The CDP model, initially proposed by Lubliner et al. [28] and further developed by Lee and Fenves [29], combines scalar damaged elasticity with non-associated compressive and tensile plasticity to accurately capture the nonlinear deformation and irreversible damage of plain concrete and FRC under various loading conditions.

The CDP model has been refined over time to incorporate the fiber effect, allowing for the analysis of FRC's mechanical behavior with minor modifications. In this study, the modified CDP model proposed by Chi et al. [12] was utilized.

2. 4. Damage Evolution Law For simplicity, this study used the model proposed by Chi et al. [12]. It can be used for different FRCs, and is easily calibrated with experimental results.

$$d_t = \frac{1}{e^{-\frac{1}{m_t}}-1}\left(e^{-\frac{\varepsilon_{t,nom}^{ck}}{m_t}} - 1\right) \quad (17)$$

$$d_c = \frac{1}{e^{-\frac{1}{m_c}}-1}\left(e^{-\frac{\varepsilon_{c,nom}^{in}}{m_c}} - 1\right) \quad (18)$$

$$\varepsilon_{t,nom}^{ck} = \frac{\varepsilon_t^{ck}}{\varepsilon_{tu}^{ck}} \quad (19)$$

$$\varepsilon_{c,nom}^{in} = \frac{\varepsilon_c^{in}}{\varepsilon_{cu}^{in}} \quad (20)$$

d_c, d_t are the uniaxial compressive and tensile damage variables. m_c,m_t, are the parameters that control damage evolution speed. $\varepsilon_{t,nom}^{ck}$, $\varepsilon_{c,nom}^{in}$denote the normalized compressive and tensile inelastic strains.
ε_{tu}^{ck},ε_{cu}^{in}, are the corresponding ultimate strains.

Typically, for plain concrete, Chi et al. [12] suggested the use of $m_t = 0{,}05$, $m_c = 0{,}1$, $\varepsilon_{cu}^{in} = 0{,}033$, $\varepsilon_{tu}^{ck} = 0{,}0033$.

The fitting of the uniaxial tension and compression simulations with experimental test data yield the exact values of m_t and m_c. For FRC, parameters m_c^{hf} and m_t^{hf} are modified according to the composite material theory as follows:

$$m_c^{hf} = m_c\left(1 + a_{m1}\lambda_{sf} + b_{m1}\lambda_{pf}\right) \quad (21)$$

$$m_t^{hf} = m_t\left(1 + a_{m2}\lambda_{sf} + b_{m2}\lambda_{pf}\right) \quad (22)$$

where λ_{sf} and λ_{pf} are the characteristic parameters of steel and polypropylene fibers, respectively.

In general, the volume fraction recommended for steel fibers is between 0.5 and 2.0 % to achieve optimal strength improvement and ductility. According to literature, an aspect ratio of 30–80, and a volume fraction of 0.05–0.2% are recommended for polypropylene fibers, to ensure even distribution of fibers [30].

The values am1 = 0.452, bm1 = 0.054, am2 = 0.628, and bm2 = 0.156 were recommended by Chi et al. [12]. The damage evolution law of the FRC specimens are shown in Figure 1.

2. 5. Parameter K_c^{hf} In the case of low hydrostatic stresses, the value Kc = 2/3 presents a close estimation of strength. However, for high hydrostatic stresses, a value of Kc = 0.7 is considered more appropriate [30].

Observations made by Chi et al. [30] indicate that the main effect on the compressive meridian is influenced by

steel fibers, unlike polypropylene fibers. Steel fibers are more effective in reducing crack propagation compared to polypropylene fibers. As a result, the tensile meridian experiences significant changes compared to the compressive meridian. Therefore, the coefficient Kc is expressed as follows:

$$K_c^{hf} = K_c.\frac{k_t}{k_c} \tag{23}$$

where kc and kt are parameters introduced to account for the presence of fibers, as suggested by Rousakis et al. [31].

$$k_t = 1 + 0{,}080\lambda_{sf} + 0{,}132\lambda_{pf} \tag{24}$$

$$k_c = 1 + 0{,}056\lambda_{sf} \tag{25}$$

$$\lambda_{sf} = V_{sf}\frac{l_{sf}}{d_{sf}} \tag{26}$$

$$\lambda_{pf} = V_{pf}\frac{l_{pf}}{d_{pf}} \tag{27}$$

2. 6. Parameter $\sigma_{b0}^{hf}/\sigma_{c0}^{hf}$ Equation (28) is recommended for low hydrostatic stress, whereas the default value of $\sigma_{b0}^{hf}/\sigma_{c0}^{hf} = 1.16$ can estimate well the strength under high hydrostatic stresses.

$$\frac{\sigma_{b0}^{hf}}{\sigma_{c0}^{hf}} = \frac{{k_t}^2}{0{,}132k_c}\left[\left(0{,}728 - \frac{0{,}749}{k_t}\right) + \sqrt{\left(0{,}728 - \frac{0{,}749}{k_t}\right)^2 + \frac{0{,}03}{{k_t}^2}}\right] \tag{28}$$

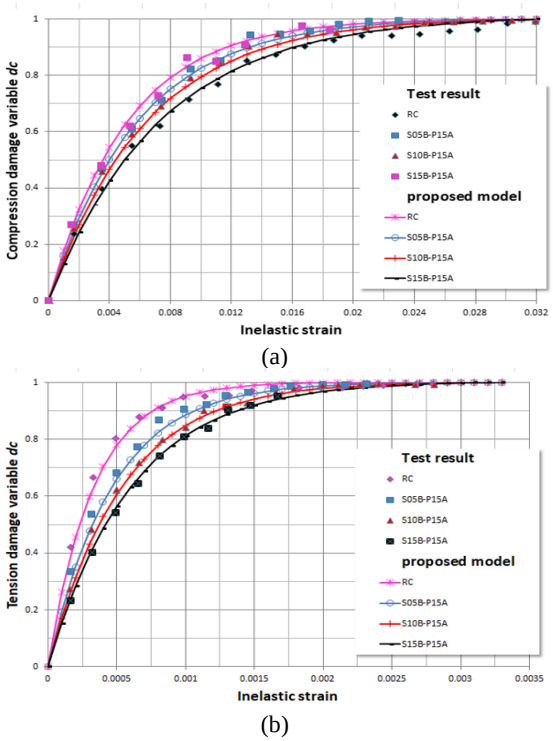

Figure 1. Damage evolution: a) compression b) tension [12]

2. 7. Dilation Angle ψ^{hf} Note that introducing fibers into the concrete matrix helps decrease the volumetric deformation rate (dilation rate), which is attributed to the confinement effect of the fibers. A decrease in the dilation angle reflects this reduction in the volumetric strain rate with increasing fiber characteristics and volume. The following relationship was presented by Chi et al. [12]:

$$\psi^{hf} = \psi_0(1 - a_\psi\lambda_{sf} - b_\psi\lambda_{pf}) \tag{29}$$

In the proposed model, the dilation angle (ψ_0) for plain concrete is determined based on the formulation proposed by Melenk and Babuška [32] and is expressed as follows:

$$\psi_0 = 36 + (\sigma_{c0}/\sigma_{cm0}) \tag{30}$$

In this equation, σ_{c0} is a parameter that ensures the equivalence of units, and σ_{cm0} is recommended to be 10 MPa according to Rousakis et al. [31]. The coefficients a_ψ and b_ψ, which are obtained from literature [12], have values of 0.861 and 0.097, respectively. These coefficients are used to calculate the dilation angle for plain concrete in the proposed model.

2. 8. Concrete Crack Evolution Law The traditional finite element methods (FEM) typically require cracks to follow element edges or predefined paths, such as cohesive zone models. However, the XFEM overcomes this limitation by allowing cracks to form independent of the model mesh, without the need for a predefined crack path. The XFEM incorporates local enrichment functions into the finite element approximation using the partition of unity method, as developed by Melenk and Babuška [32]. Additionally, this study enhances the XFEM by incorporating the generalized Heaviside function [33], simplifying the treatment of arbitrarily curved cracks without complex mapping.

In this study, the evolution of cracks in concrete is determined using the displacement parameter and Equations (8) and (12) as described in this paper. The XFEM is implemented in the Abaqus Implicit software to simulate the process of concrete cracking. The specific parameters used for the XFEM implementation can be found in Table 1.

The proposed approach in this study is a coupled XFEM-CDP model for FRC columns. The flowchart of the implicit simulation scheme used in this study is illustrated in Figure 2.

2. 9. Steel Material Model The reinforcing steel bars in the concrete columns were represented using truss elements (T3D2) in the analysis. These truss elements were assumed to exhibit linear elastic behavior. The material model for the steel bars involved linear hardening until they reached the ultimate stress in tension

TABLE 1. XFEM parameters

	RC	FRC
Crack initiation	ft	a1*ftFRC
Crack evolution law	Exponential	Exponential
Evolution law parameter	c1/wcr	a2
Displacement at failure	wcr	2/a2

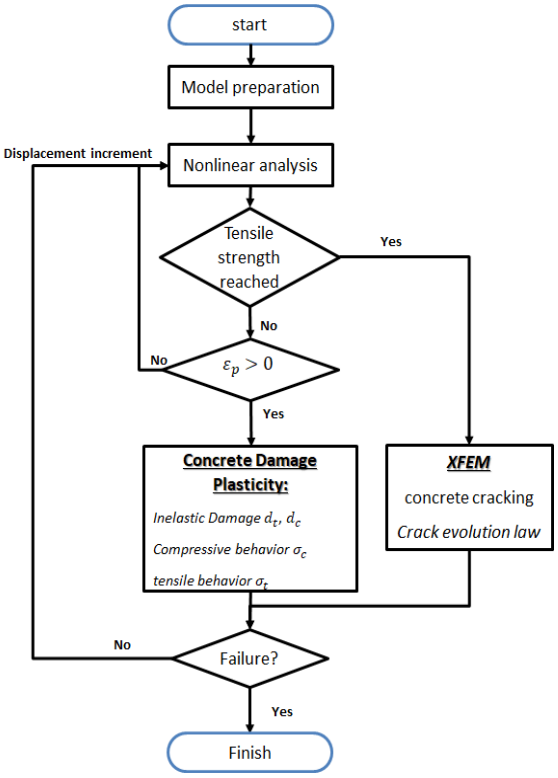

Figure 2. Flowchart of the coupled XFEM and concrete damage plasticity

(σ_su). Subsequently, the strain-softening behavior of the bars was simulated in Abaqus using the damage fracture option.

To calibrate the model with test results, the estimated displacement at failure (wf) was determined. This calibration process is depicted in Figure 3.

Table 2 provides a summary of the mechanical properties incorporated in the material model for the reinforcing steel. These properties include parameters such as the yield strength, ultimate strength, elastic modulus, and fracture displacement. These properties are essential for accurately capturing the behavior of the reinforcing steel bars in the numerical simulations.

3. RESULTS AND DISCUSSIONS

3. 1. Model Validation with Experimental Results

Simulations were conducted in Abaqus using quasi-static cyclic pushover analysis. Finite element models of columns with various RC and FRC materials were calibrated and validated using experimental data from previous studies [2, 12-14]. Table 3 summarizes the main parameters for the different FRC columns.

Constitutive models of steel bars and concrete matrix components were separately established for numerical modeling. Stirrups were modeled using truss elements (T3D2), and the concrete matrix was assigned a solid three-dimensional eight-node linear brick with full integration (C3D8). Note that the XFEM converges faster with full integration elements C3D8 than with reduced integration elements (C3D8R).

Figures 4-9 depict the hysteretic curves of eight different types of RC, SFRC, PFRC and HyFRC columns, with the solid black line representing experimental results and the dash red line representing numerical simulation results. It can be seen that the cyclic

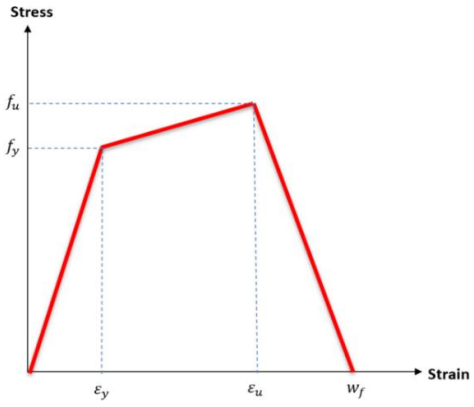

Figure 3. Reinforcing steel model for steel bars

TABLE 2. Steel parameters for different models

Model	d (mm)	fy (MPa)	fu (MPa)	Es (MPa)	εh	εu
(a) Zhang et al. [2]	10	335	500	$2.0*10^5$	0.001675	0.06
(b) Zhang, et al. [10]	14	335	500	$2.0*10^5$	0.001675	0.06
(c) Huang et al. [8]	14	553.9	670.3	$2.0*10^5$	0.001675	0.06
(d) Liang et al. [9]	16	440	609	$1.95*10^5$	0.001675	0.08

TABLE 3. Values for CPDM for (a, b, c, d) normal RC, (e, f, g) SFRC, (h) PFRC and (i) HYFRC

Sample	Vsf (%)	Vpf (%)	ψ (°)	$\sigma_{b0}^{hf}/\sigma_{c0}^{hf}$	K	Mesh size (mm)
(a). RC-Zhang et al. [2]	0.0	0.0	38.70	1.162	0.666	77
(b). RC-Zhang et al. [10]	0.0	0.0	38.70	1.162	0.666	50
(c). RC-Huang et al. [8]	0.0	0.0	38.70	1.162	0.666	40
(d). RC-Liang et al. [9]	0.0	0.0	38.70	1.162	0.666	60
(e). SFRC-Zhang et al. [2]	1.0	0.0	16.775	1.46	0.676	77
(f). SFRC-Zhang et al. [10]	1.0	0.0	16.775	1.46	0.676	50
(g). SFRC-Zhang et al. [10]	1.5	0.0	6.609	1.634	0.681	50
(h). PF-1-1-Huang et al. [8]	0.0	0.15	34.968	1.162	0.718	40
(i). HF-1-1-Huang et al. [8]	1.5	0.15	4.085	1.641	0.731	40

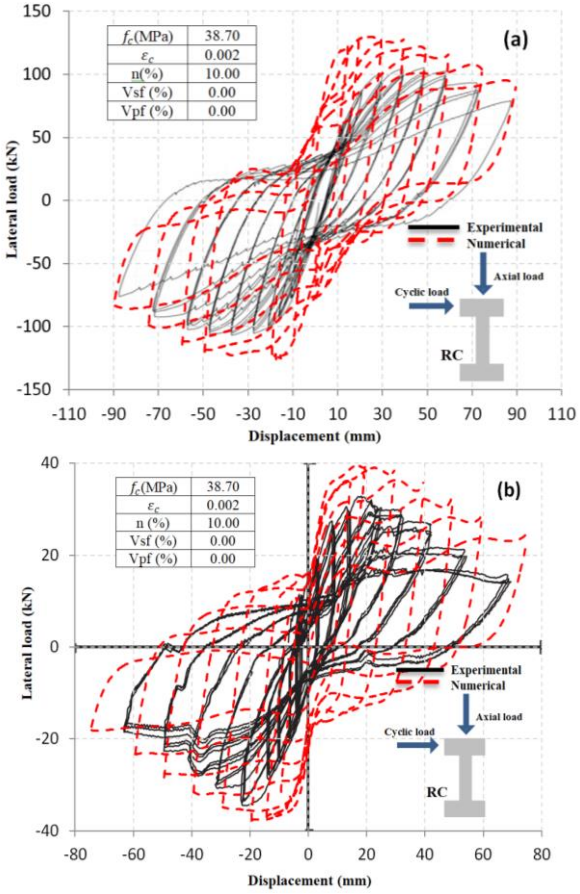

Figure 4. Comparison of the numerical hysteresis curve of RC columns with the experimental hysteresis response curves from: a) [2], b) [10]

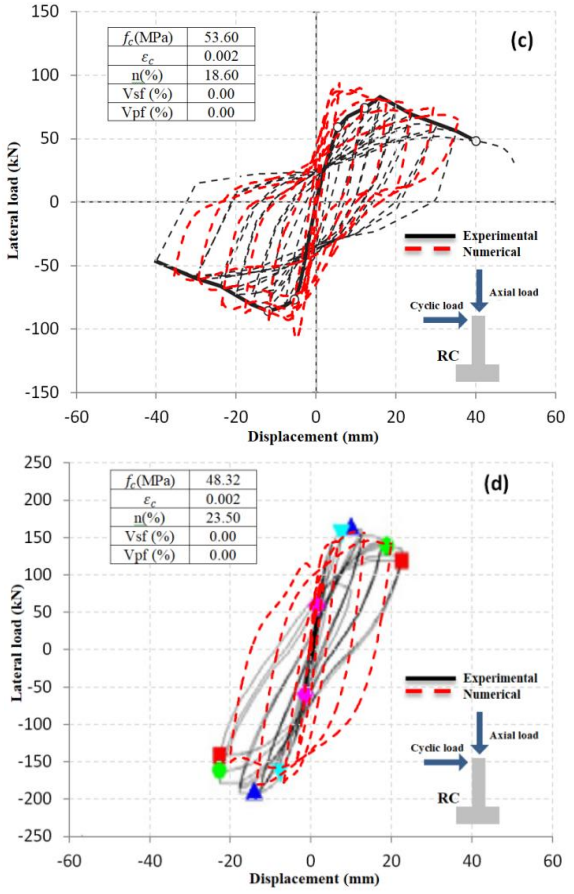

Figure 5. Comparison of the numerical hysteresis curve of RC columns with the experimental hysteresis response curves from: c) [8], d) [9]

deterioration of these columns' performance (i.e., the gradual decrease of stiffness, the loss of strength due to cyclic loading, and the pinched form caused by concrete cracking).

The comparison results in Figures 10-15 show that the dynamic hysteretic model can provide reasonable estimates of the strength capacity of various FRC columns. Furthermore, the proposed degradation parameters accurately depict the deterioration of strength and stiffness, as well as the pinching effect.

The analytical models SFRC-Zhang and RC-Zhang et al. [2] showed the most significant difference between the test results and the predicted load, 134 and 436 %, respectively. This error was primarily due to the large

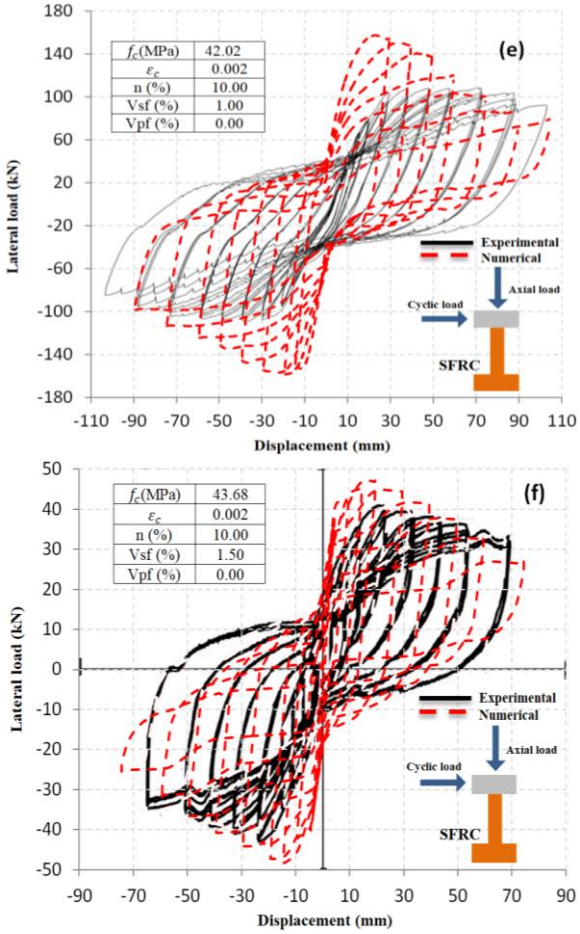

Figure 6. Comparison of the numerical hysteresis curve of SFRC columns with the experimental hysteresis response curves from: a) [2], b) [14]

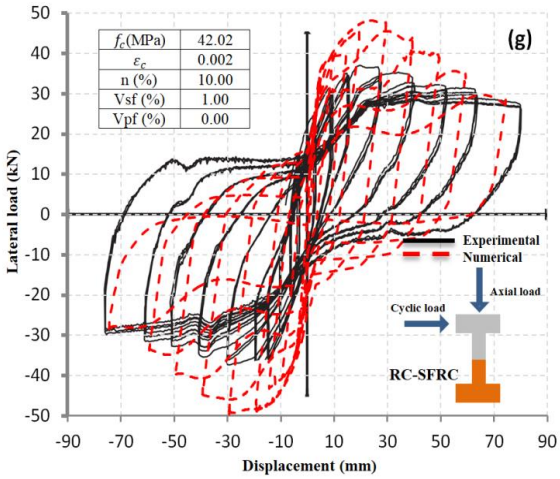

Figure 7. Comparison of the numerical hysteresis curve of RC-SFRC columns with the experimental hysteresis response curves from [10]

mesh size used in these models (which is 77 mm as shown in Table 3). More significant errors in the lateral

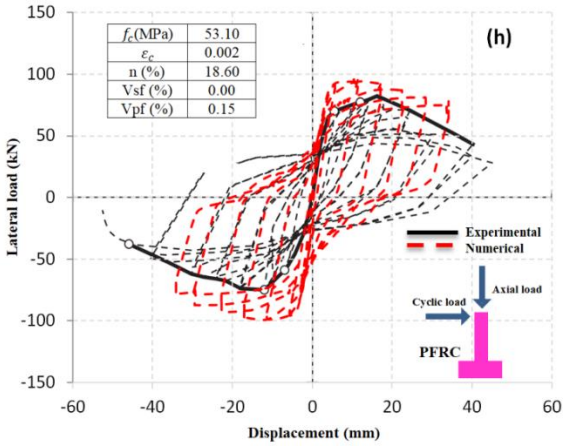

Figure 8. Comparison of the numerical hysteresis curve of PFRC columns with the experimental hysteresis response curves from [8]

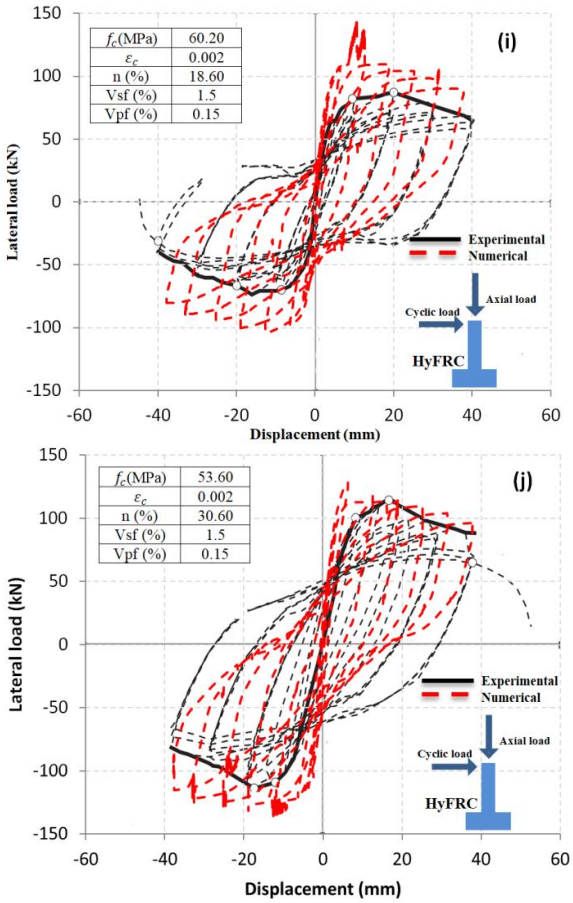

Figure 9. Comparison of the numerical hysteresis curve of HyFRC columns with the experimental hysteresis response curves from [8]

loads occurred at smaller displacements because larger mesh elements require higher fracture energies. This highlights the importance of mesh size sensitivity analysis.

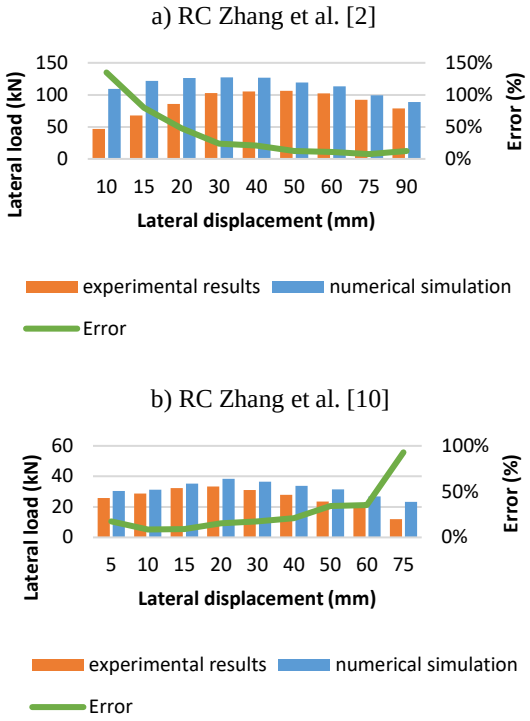

Figure 10. Comparison of numerical results for RC columns with experimental results from: a) [2], b) [14]

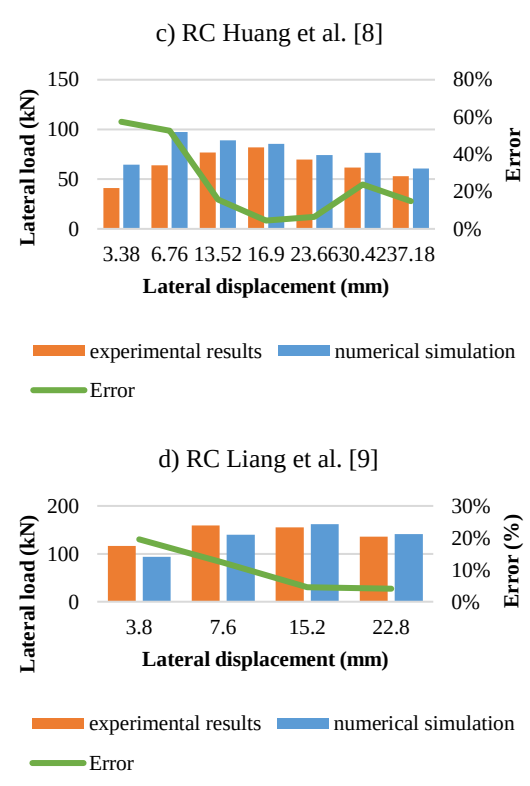

Figure 11. Comparison of numerical results for RC columns with experimental results from: c) [2], d) [14]

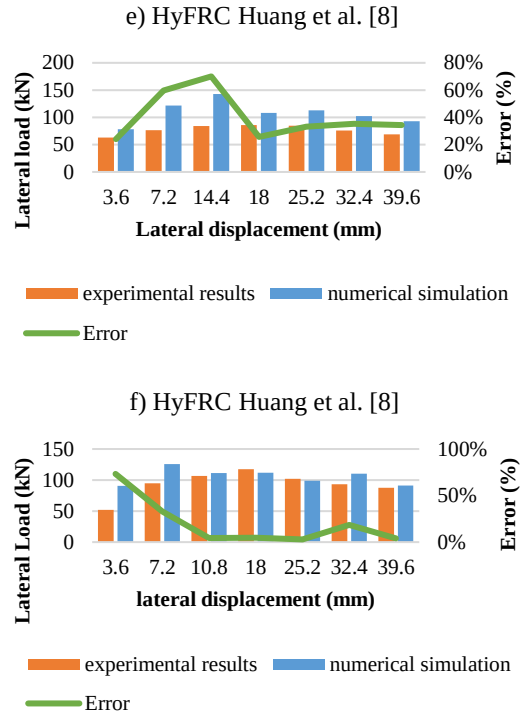

Figure 12. Comparison of numerical results for SFRC columns with experimental results from [2]

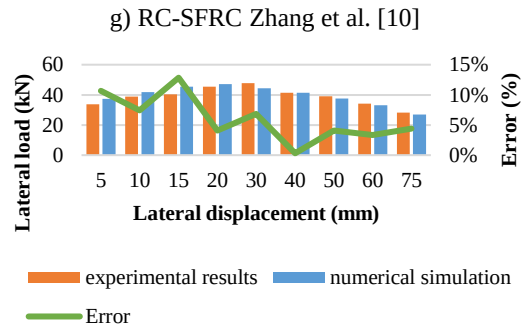

Figure 13. Comparison of numerical results for RC-SFRC columns with experimental from [8]

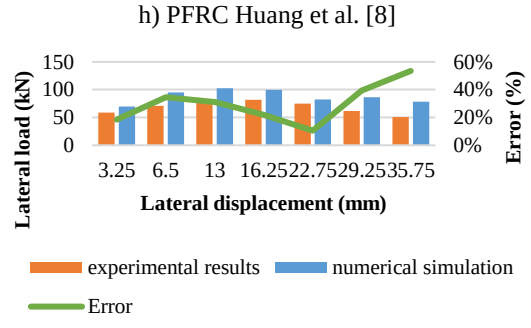

Figure 14. Comparison of numerical results for PFRC columns with experimental from [8]

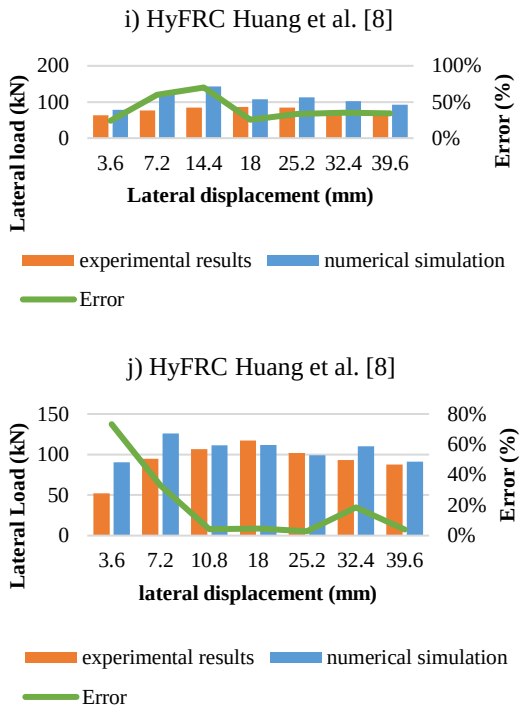

Figure 15. Comparison of numerical results for HyFRC columns with experimental results from [2]

3. 2. Mesh Sensitivity Analysis A mesh sensitivity study should be performed before performing a detailed finite element analysis. Three element sizes (25, 40, and 50 mm) were adopted to investigate the effect of the mesh size on the cyclic behavior of the FRC columns, as shown in Figures 16 and 17.

Figure 18 depicts a comparison of different element sizes along with the experimental test results for SFRC column from Broumand and Khoei [14], to investigate the effect of mesh size on accuracy. It can be observed that the load-displacement curve accurately traced the corresponding experimental results. Fine meshes produced results that were very close to the experimental test results for the lateral load.

The precision of the results and computing time of finite element analysis (FEA) are highly dependent on the mesh size. According to the results shown in Table 4, it can be concluded that Fine-mesh FEA models produce more accurate results and better cracking patterns than model with coarse meshes.

On the other hand, models with coarse meshes produce less accurate results, but they save computing time by reducing the model size. These simplified models are typically used to provide rough but rapid analysis estimation.

3. 2. Comparison of CDP model And Combined XFEM/CDP Figure 19 compares the simulation results and experimental data from previous studies [10]. In addition, a CDP model that excludes the matrix cracking effect was also used for comparison. Both models accurately predict the ultimate lateral force and skeleton curve.

However, when it comes to the unloading stiffness, the CDP model alone fails to reproduce the degradation law observed in the experimental curves. On the other hand, the proposed model, which combines the XFEM with the CDP model, can reasonably reflect the pinch effect observed in the experimental results. This is mainly attributed to the incorporation of cracking and

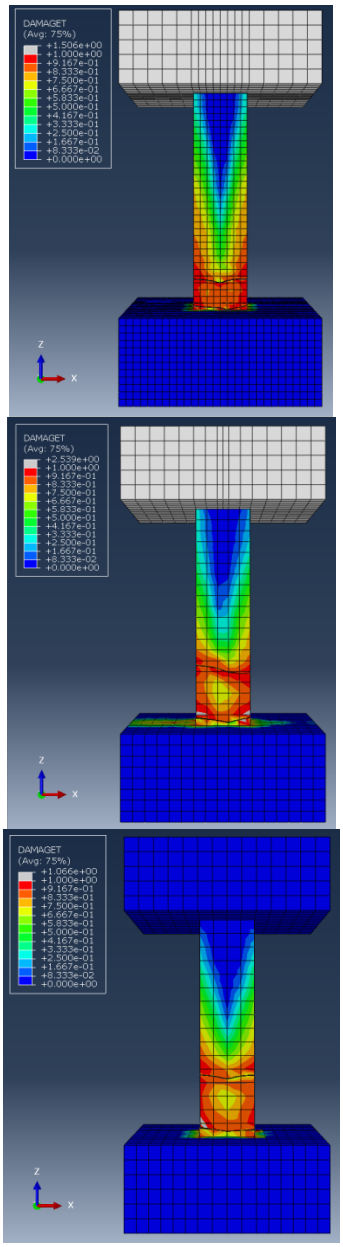

Figure 16. Tensile damage results for different mesh sizes: a) 25 mm, b) 40 mm, c) 50 mm

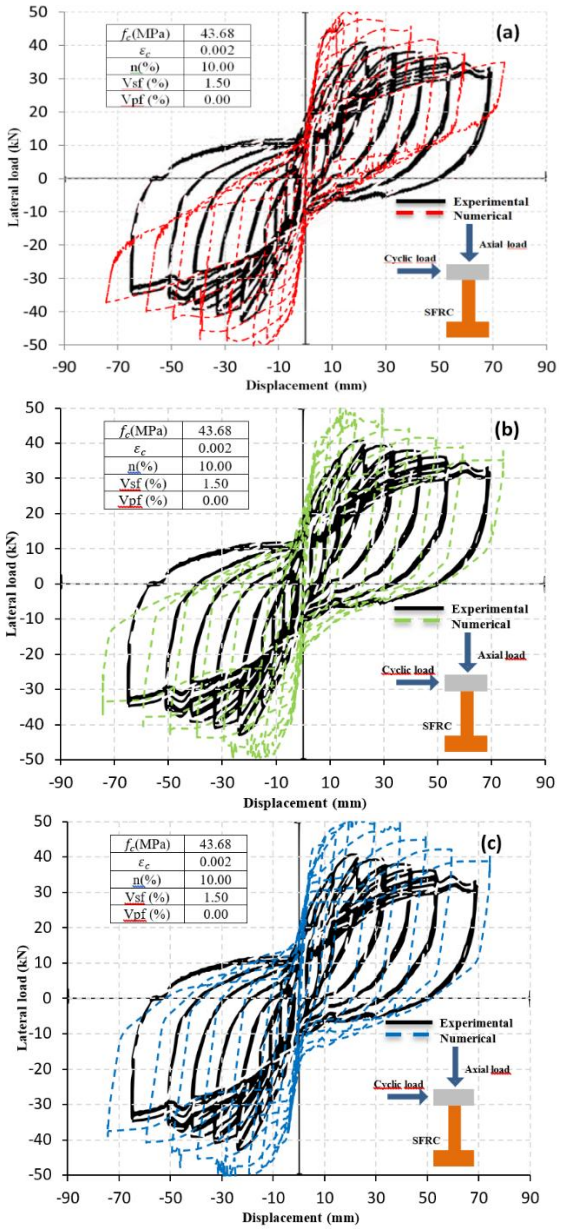

Figure 17. Comparison of Hysteresis curves of SFRC column for different mesh sizes: a) 25 mm, b) 40 mm and c) 50 mm

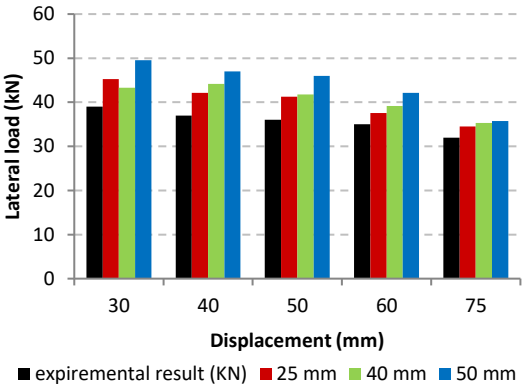

Figure 18. Comparison between the numerical and experimental load values of SFRC column [8] for different mesh sizes: 25 mm, 40 mm and 50 mm

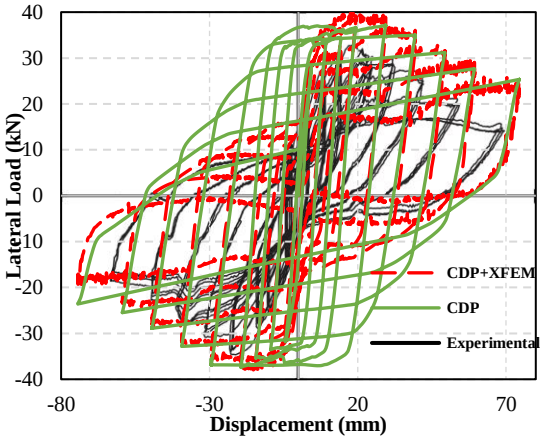

Figure 19. Comparison Comparison of CDP model and combined XFEM-CDP for RC [8]

crack closing behavior during unloading, which leads to the formation of pinched hysteresis loops. In contrast, simulations based solely on the CDP model tend to produce plump hysteresis loops that do not capture the observed behavior accurately.

TABLE 4. Mesh sensitivity analysis results

Lateral displacement (mm)	Experimental result (kN)	Analytical result					
		25 mm		40 mm		50 mm	
		lateral force (kN)	Variation (%)	lateral force (kN)	Variation (%)	lateral force (kN)	Variation (%)
30	39	45.23	24%	43.30	11%	49.55	27%
40	37	42.12	14%	44.17	19%	47.02	27%
50	36	41.26	15%	41.78	16%	45.95	28%
60	35	37.56	7%	39.18	12%	42.10	20%
75	32	34.47	8%	35.32	10%	35.72	12%

4. CONCLUSION

This paper proposes an Abaqus-based method for combining the CDP model with the XFEM for FRC structures, to more realistically reproduce the mechanical responses of FRC. The following conclusions can be presented:

- The proposed coupled (XFEM+CDP) model has been successfully validated using independent experimental results with variations in mesh sizes, material properties, and structural scales. This validation ensures the reliability and applicability of the model.
- The numerical investigation of mesh size sensitivity reveals that the accuracy of the proposed model is dependent on the element size. Proper selection of element size is crucial to achieve accurate results.
- The proposed model demonstrates improved agreement with experimental data compared to classical CDP models. It effectively captures the pinched form of hysteresis loops of concrete under cyclic loadings, providing a more realistic representation of FRC behavior.
- The agreement between the experimental results and numerical predictions provides strong evidence supporting the relevance and effectiveness of the proposed model.

This model can serve as a valuable tool for conducting nonlinear and dynamic numerical simulations of reinforced concrete (RC) and FRC structures using Abaqus software, providing valuable guidelines for practical applications in structural engineering.

5. REFERENCES

1. Opabola, E. A., and Mangalathu, S. "Seismic fragility assessment of bridges with as-built and retrofitted splice-deficient columns." ***Bulletin of Earthquake Engineering***, Vol. 21, No. 1, (2023), 583-603. https://doi.org/10.1007/s10518-022-01521-w
2. Zhang, Y. Y., Harries, K. A., and Yuan, W. C. "Experimental and numerical investigation of the seismic performance of hollow rectangular bridge piers constructed with and without steel fiber reinforced concrete." ***Engineering Structures***, Vol. 48, (2013), 255-265. https://doi.org/10.1016/j.engstruct.2012.09.040
3. Marc-André, D., and Bruno, M. "Tension Lap Splices Strengthened with Ultrahigh-Performance Fiber-Reinforced Concrete." ***Journal of Materials in Civil Engineering***, Vol. 27, No. 7, (2015), 4014206. https://doi.org/10.1061/(ASCE)MT.1943-5533.0001169
4. Hajsadeghi, M., Jalali, M., Chin, C. S., Zirakian, T., and Bahrebar, M. "Flexural Performance of Fibre Reinforced Concrete with an Optimised Spirally Deformed Steel Fibre." ***International Journal of Engineering, Transactions C: Aspects***, Vol. 34, No. 6, (2021), 1390-1397. https://doi.org/10.5829/ije.2021.34.06c.01
5. Rahmanzadeh, S., and Tariverdilo, S. "Evaluating Applicability of ASTM C 928 Approach in Assessing Adequacy of Patch Repair of Bridge Piers." ***International Journal of Engineering Transactions C: Aspects***, Vol. 33, No. 12, (2020), 2455-2463. https://doi.org/10.5829/ije.2020.33.12c.04
6. Magbool, H. M., and Zeyad, A. M. "The effect of various steel fibers and volcanic pumice powder on fracture characteristics of Self-Compacting concrete." ***Construction and Building Materials***, Vol. 312, (2021), 125444. https://doi.org/https://doi.org/10.1016/j.conbuildmat.2021.125444
7. Zhang, P., Wei, S., Wu, J., Zhang, Y., and Zheng, Y. "Investigation of mechanical properties of PVA fiber-reinforced cementitious composites under the coupling effect of wet-thermal and chloride salt environment." ***Case Studies in Construction Materials***, (2022).
8. Huang, L., Xu, L., Chi, Y., and Xu, H. "Experimental investigation on the seismic performance of steel-polypropylene hybrid fiber reinforced concrete columns." ***Construction and Building Materials***, Vol. 87, (2015), 16-27. https://doi.org/10.1016/j.conbuildmat.2015.03.073
9. Liang, X., Xing, P., and Xu, J. "Experimental and numerical investigations of the seismic performance of columns with fiber-reinforced concrete in the plastic hinge region." ***Advances in Structural Engineering***, Vol. 19, No. 9, (2016), 1484-1499. https://doi.org/10.1177/1369433216643896
10. Zhang, Y., and Dias-da-Costa, D. "Seismic vulnerability of multi-span continuous girder bridges with steel fibre reinforced concrete columns." ***Engineering Structures***, Vol. 150, (2017), 451-464. https://doi.org/10.1016/j.engstruct.2017.07.053
11. Pang, Y., Cai, L., Ouyang, H., and Zhou, X. "Seismic performance assessment of different fibers reinforced concrete columns using incremental dynamic analysis." ***Construction and Building Materials***, Vol. 203, (2019), 241-257. https://doi.org/10.1016/j.conbuildmat.2019.01.087
12. Chi, Y., Yu, M., Huang, L., and Xu, L. "Finite element modeling of steel-polypropylene hybrid fiber reinforced concrete using modified concrete damaged plasticity." ***Engineering Structures***, Vol. 148, (2017), 23-35. https://doi.org/10.1016/j.engstruct.2017.06.039
13. Aljazaeri, Z. R., and Al-Jaberi, Z. "Numerical Study on Flexural Behavior of Concrete Beams Strengthened with Fiber Reinforced Cementitious Matrix Considering Different Concrete Compressive Strength and Steel Reinforcement Ratio." ***International Journal of Engineering Transactions A: Basics***, Vol. 34, No. 4, (2021), 793-802. https://doi.org/10.5829/ije.2021.34.04a.05
14. Broumand, P., and Khoei, A. R. "X-FEM Modeling of Dynamic Ductile Fracture Problems with a Nonlocal Damage-Viscoplasticity Model." ***Finite Elements in Analysis and Design***, Vol. 99, No. C, (2015), 49-67. https://doi.org/10.1016/j.finel.2015.01.002
15. Sadat Hosseini, A., Hajikarimi, P., Fallah Hosseini, S., Aliakbari, A., and Moghadas Nejad, F. "Semi-circular bending setup for predicting fracture characteristics of high-strength fiber-reinforced concrete." ***Theoretical and Applied Fracture Mechanics***, Vol. 123, (2023), 103729. https://doi.org/https://doi.org/10.1016/j.tafmec.2022.103729
16. Javanmardi, M. R., and Maheri, M. R. "Extended finite element method and anisotropic damage plasticity for modelling crack propagation in concrete." ***Finite Elements in Analysis and Design***, Vol. 165, (2019), 1-20. https://doi.org/https://doi.org/10.1016/j.finel.2019.07.004
17. Belletti, B., Cerioni, R., Meda, A., and Plizzari, G. "Design Aspects on Steel Fiber-Reinforced Concrete Pavements." ***Journal of Materials in Civil Engineering***, Vol. 20, (2008). https://doi.org/10.1061/(ASCE)0899-1561(2008)20:9(599)
18. Prisco, M., Dozio, D., and Belletti, B. "On the fracture behaviour

of thin-walled SFRC roof elements." ***Materials and Structures***, Vol. 46, No. 5, (2013), 803-829. https://doi.org/10.1617/s11527-012-9935-x

19. Ren, X., and Li, J. "Multi-scale based fracture and damage analysis of steel fiber reinforced concrete." ***Engineering Failure Analysis***, Vol. 35, (2013), 253-261. https://doi.org/10.1016/j.engfailanal.2013.01.029
20. Zhang, H., Huang, Y., Xu, S., Natarajan, S., and Yao, F. "An explicit methodology of random fibre modelling for FRC fracture using non-conforming meshes and cohesive interface elements." ***Composite Structures***, Vol. 310, (2023), 116762. https://doi.org/https://doi.org/10.1016/j.compstruct.2023.116762
21. Rabczuk, T., and Belytschko, T. "Cracking particles: a simplified meshfree method for arbitrary evolving cracks." ***International Journal for Numerical Methods in Engineering***, Vol. 61, No. 13, (2004), 2316-2343. https://doi.org/https://doi.org/10.1002/nme.1151
22. Moslemi, H., and Khoei, A. R. "3D adaptive finite element modeling of non-planar curved crack growth using the weighted superconvergent patch recovery method." ***Engineering Fracture Mechanics***, Vol. 76, No. 11, (2009), 1703-1728. https://doi.org/https://doi.org/10.1016/j.engfracmech.2009.03.013
23. De Maio, U., Greco, F., Leonetti, L., Nevone Blasi, P., and Pranno, A. "A cohesive fracture model for predicting crack spacing and crack width in reinforced concrete structures." ***Engineering Failure Analysis***, Vol. 139, (2022), 106452. https://doi.org/https://doi.org/10.1016/j.engfailanal.2022.106452
24. Kurumatani, M., Soma, Y., and Terada, K. "Simulations of cohesive fracture behavior of reinforced concrete by a fracture-mechanics-based damage model." ***Engineering Fracture Mechanics***, Vol. 206, (2018). https://doi.org/10.1016/j.engfracmech.2018.12.006
25. Fallah, N. "A development in the finite volume method for the crack growth analysis without global remeshing." ***International Journal of Engineering, Transactions A: Basics***, Vol. 29, No. 7, (2016), 898-908. Retrieved from doi: 10.5829/idosi.ije.2016.29.07a.03
26. Abadel, A., Abbas, H., Almusallam, T., Al-Salloum, Y., and Siddiqui, N. "Mechanical properties of hybrid fibre-reinforced concrete – analytical modelling and experimental behaviour." ***Magazine of Concrete Research***, Vol. 68, No. 16, (2016), 823-843. https://doi.org/10.1680/jmacr.15.00276
27. Almusallam, T., Ibrahim, S. M., Al-Salloum, Y., Abadel, A., and Abbas, H. "Analytical and experimental investigations on the fracture behavior of hybrid fiber reinforced concrete." ***Cement and Concrete Composites***, Vol. 74, (2016), 201-217. https://doi.org/10.1016/j.cemconcomp.2016.10.002
28. Lubliner, J., Oliver, J., Oller, S., and Oñate, E. "A plastic-damage model for concrete." ***International Journal of Solids and Structures***, Vol. 25, No. 3, (1989), 299-326. https://doi.org/10.1016/0020-7683(89)90050-4
29. Lee, J., and Fenves, G. L. "Plastic-Damage Model for Cyclic Loading of Concrete Structures." ***Journal of Engineering Mechanics***, Vol. 124, No. 8, (1998), 892-900. https://doi.org/10.1061/(asce)0733-9399(1998)124:8(892)
30. Chi, Y., Xu, L., and Yu, H. sui. "Constitutive modeling of steel-polypropylene hybrid fiber reinforced concrete using a non-associated plasticity and its numerical implementation." ***Composite Structures***, Vol. 111, No. 1, (2014), 497-509. https://doi.org/10.1016/j.compstruct.2014.01.025
31. Rousakis, T. C., Karabinis, A. I., Kiousis, P. D., and Tepfers, R. "Analytical modelling of plastic behaviour of uniformly FRP confined concrete members." ***Composites Part B: Engineering***, Vol. 39, No. 7-8, (2008), 1104-1113. https://doi.org/10.1016/J.COMPOSITESB.2008.05.001
32. Melenk, J. M., and Babuška, I. "The partition of unity finite element method: Basic theory and applications." ***Computer Methods in Applied Mechanics and Engineering***, Vol. 139, No. 1-4, (1996), 289-314. https://doi.org/10.1016/S0045-7825(96)01087-0
33. Moes, N., Dolbow, J., and Belytschko, T. "A Finite Element Method for Crack Growth without Remeshing." ***International Journal for Numerical Methods in Engineering***, Vol. 46, , (1999), 131-150. https://doi.org/10.1002/(SICI)1097-0207(19990910)46:13.0.CO;2-J

Persian Abstract

چکیده

در سال‌های اخیر، جامعه علمی علاقه فزاینده‌ای به بتن تقویت‌شده با الیاف (FRC)برای سازه‌های مدرن به دلیل شکل‌پذیری افزایش یافته آن در مقایسه با بتن مسلح سنتی (RC)نشان داده است. این مقاله یک مدل تحلیلی را معرفی می‌کند که شامل یک شاخص تقویت‌کننده فیبر جامع (RI)برای مطالعه انواع مختلف FRC است. تجزیه و تحلیل بر روی رفتارهای فشاری و کششی، تکامل آسیب تحت بارگذاری چرخه ای، و انتشار ترک در زمینه بتن متمرکز است. برای شبیه‌سازی موثر شروع و انتشار ترک در سازه‌های FRC، از روش المان محدود توسعه‌یافته (XFEM)استفاده می‌شود که از قابلیت‌های حل شکست آن استفاده می‌کند. علاوه بر این، XFEM با رویکرد مدل‌سازی پلاستیسیته آسیب‌دیده بتن (CDP)ترکیب می‌شود تا عملکرد شبه استاتیک و هیسترتیک ستون‌های FRC را بررسی کند. مدل های المان محدود غیرخطی سه بعدی با استفاده از نرم افزار تجاری Abaqus ساخته شده اند. این مدل ها از الیاف فولادی، الیاف پلی پروپیلن و ترکیبی از هر دو نوع الیاف در ساختارهای FRC استفاده می کنند. علاوه بر این، دقت تجزیه و تحلیل مبتنی بر XFEM-CDP در پیش‌بینی رفتار هیسترتیک در برابر نتایج مقالات تحقیقاتی قبلی تأیید می‌شود و دقت معقولی را نشان می‌دهد. این به مهندسان اجازه می دهد تا رفتار غیرخطی بتن، از جمله ترک خوردگی، خرد شدن، و تغییر شکل پلاستیک را به طور دقیق ثبت کنند، در حالی که الگوهای ترک پیچیده را نیز در نظر می گیرند و درک بهتری از عملکرد لرزه ای سازه های FRC با استفاده از شبیه سازی های عددی ارائه می دهند.